Evaluation of Processing Effects in Injection-Molded Amorphous and Crystalline Thermoplastics Using an Excimer Laser

E. Sancaktar, N. Negandhi, S. Adwani

Department of Polymer Engineering, University of Akron, Akron, Ohio 44325-0301

Received 7 March 2005; accepted 25 September 2005
DOI 10.1002/app.23281
Published online in Wiley InterScience (www.interscience.wiley.com).

ABSTRACT: The ablation behavior of amorphous [polystyrene (PS), polycarbonate (PC)] and crystalline [PET, glass-filled poly(butylene terephthalate) (PBT)] polymers by 248-nm KrF excimer laser irradiation were investigated for different injection-molding conditions, namely, injection flow rate, injection pressure, and mold temperature, as a possible method for evaluating processing effects in the specimens. For this purpose, dumbbell-shaped samples were injection-molded under different sets of processing conditions, and weight loss measurements were carried out for the different injection-molding conditions. Some of the crystalline (PET) samples were annealed at different annealing times and temperatures. For PET, the weight loss decreased with increasing mold temperature and remained insensitive to injection flow rate. Annealing time and temperature significantly reduced weight loss in PET. For PBT, the weight loss due to laser ablation decreased with increasing material packing due to pressure, and it also showed some sensitivity to flow rate variation. The major effect was seen with glass-filled PBT samples. The weight loss decreased drastically with increasing glass fiber content. Laser ablation allowed us to observe process-induced fiber orientation by scanning electron microscopy in PBT samples. For PS and PC, the weight loss increased with increasing injection flow rate and mold temperature and decreased with increasing injection pressure. The position near the gate showed higher ablation than the position at the end for all the conditions. A decrease in the material orientation with injection speed and mold temperature led to an increase in the weight loss, whereas an increase in the injection pressure, and consequently orientation, led to a lower weight loss for PS and PC. Higher residual stress samples showed higher weight losses. J Appl Polym Sci 101: 258–268, 2006

Key words: injection molding; laser ablation; fibers; orientation; structure-property relations

INTRODUCTION

In today's industry, injection molding is one of the most important processing methods for the high-volume manufacturing of identical parts. More than 30% of the final products manufactured from thermoplastics are made by injection molding. Injection molding is a versatile process that can be used to mold extremely complex shapes, large and small parts, and articles with metal inserts and can have very low cycle times. Being an intermittent cyclic process, it is used to shape all classes of thermoplastics, thermosets, and rubbers. Present-day automation has helped to manufacture injection-molded parts with no flash and cycle times as low as a few seconds, which makes it highly economical and reliable.

During injection molding, the polymer melt passes through complex thermomechanical processes, which highly influence the morphology of the final part. Semicrystalline polymers also experience transitions from fluid to rubbery and to crystalline states. The molding parameters, injection speed and mold temperature, have a prominent effect on the morphological features, including chain orientation, internal stresses, and percentage crystallinity. These microstructural features directly affect the performance and properties of the part.

In this study, dumbbell-shaped specimens were injection-molded under different sets of processing conditions with semicrystalline polymers, including poly(ethylene terephthalate) (PET) and poly(butylene terephthalate) (PBT). Also, sets of samples were prepared with 15 and 30% glass-filled PBT. Some PET samples were annealed at different annealing temperatures and times. All molded and annealed PET samples were analyzed for percentage crystallinity in the skin and core regions with differential scanning calorimetry (DSC). Two amorphous polymers, namely, polystyrene (PS) and polycarbonate (PC), were also studied with dumbbell-shaped injection-molded specimens under different injection-molding conditions,

Correspondence to: E. Sancaktar (erol@uakron.edu).
Contract grant sponsor: National Science Foundation; contract grant number: 9724185.

with variations in injection flow rate, injection pressure, and mold temperature in two positions: near the gate and near the end. With a novel laser irradiation procedure, weight loss measurements were made and correlated to different injection-molding conditions.

UV excimer lasers are becoming more popular day by day and are used for the processing of polymers. The interactions of UV lasers with polymers are quite complicated, and the mechanism of ablation is still under discussion. The effect of laser ablation on a polymer surface largely depends on the laser parameters and the morphology/microstructure of the polymer surface.

The injection-molding process involves complexities in mold design, barrel design, product design, and so on. The thermoplastics that are injection-molded need to be specially prepared with low melt viscosity so that they can be easily squeezed through the narrow channels of sprue, runner, and gate. Understanding how to obtain the maximum performance of each individual operation in the complete molding process and properly integrating each step to meet product performance at the lowest cost are very important. Processing parameters, such as melt temperature, injection speed, injection pressure, packing and hold-on pressure, packing and hold-on time, cooling time, mold temperature, backpressure, and screw rotation speed, all affect structure–property development during injection molding.[1–6]

Structure development in injection molding

During injection molding, the polymer experiences a very complex thermomechanical history. This history is a result of complicated molding conditions, which include nonisothermal transient flow of a non-Newtonian fluid in complex geometries with simultaneous structuring and solidification. The mold flow geometry and intrinsic material properties, such as melting temperature, crystallization temperature, rate of crystallization, heat of fusion, temperature, and shear dependence of viscosity, also play important roles.[6]

Semicrystalline polymers can be classified into two main categories depending on their crystallization kinetics:[7] (1) fast crystallizing polymers (e.g., polyethylene [PE], polypropylene [PP], polyacetal [POM]), which have microstructures that cannot be greatly influenced by the processing conditions, and (2) slow crystallizing polymers (e.g., PET, polyetheretherketone [PEEK], polyphenylene sulfide [PPS]), which have relatively rigid backbones containing aromatic groups and, thus, possess microstructures highly dependent on cooling rates.[8,9]

Structure development in semicrystalline polymers has been widely studied. The observed morphology for all fast-crystallizing polymers is a three-layered structure parallel to the flow direction, but gradients up to five layers have been reported.[5] The three distinct layers widely reported are the skin layer with chains oriented in flow direction, the shear/transcrystalline layer with a high level of shear crystallinity and orientation in the flow direction, and the core region with spherulitic structures without any specific orientation direction.[6]

Injection-molding studies of amorphous polymers have mainly focused on orientation and residual stress determination, as these factors result in highly anisotropic mechanical behavior, shrinkage, and warpage. Many authors have also investigated the effect of different processing conditions, namely, injection speed, injection pressure, melt temperature, and mold temperature, on birefringence and residual stresses. It has been found that birefringence decreases with increasing injection speed, melt temperature, and mold temperature, whereas it increases with increasing packing pressure.

Flow pattern in injection molding

The melt flow pattern during the mold-filling phase affects the microstructure of the final product. Tadmor[4] studied the flow pattern of an advancing melt front in the mold and stated that the actual shape of the advancing front was semicircular and that the fluid particles followed the free surface in a curved path until they reached the wall. Thus, the orientation of the polymer chains in the skin layer will be due to steady elongational flow, and it will be in the flow direction. The final orientation distribution in the skin layer will be a function of the cooling rate and the spectrum of relaxation times. However, at some distance from the gate, the velocity profile is close to fully developed shear flow, which leads to shear-induced orientation.

Orientation and residual stresses

As discussed previously, during injection molding, the polymer experiences a very complex thermomechanical history through fluid, rubbery, glassy, and crystallized states, which results in frozen-in stresses[4,10] and frozen-in orientation in the molded part.

With rapid cooling and solidification process, the part starts solidifying at the surface. This results in thermal stresses that are compressive near the surface and tensile in the core region. Also, during cooling, the polymer crystallizes, and this imparts densification and transitions in viscoelastic behavior of the material. The simultaneous existence of amorphous zones and crystallites creates more complications due to inherent thermal and stress behavior differences between the two phases. The thermal gradients in thickness and flow direction impart anisotropy in crystal growth

over the specimen, which results in shrinkage and warpage.

Experimental techniques for detecting the presence of residual stresses have been studied by many authors. There are basically five techniques used: (1) the solvent crazing technique,[11,12] (2) the nondestructive photoelastic frozen stress technique,[13] (3) the hole-drilling method,[14,15] (4) the material removal method,[16] and (5) holographic interferometry.[16] All of these conventional methods are very limited in their ability to measure residual stresses in nontransparent plastic parts.

The effect of the filling process on molecular orientation has been widely discussed in the literature.[10,14,15,17,18] The skin layer is very thin and is formed when the polymer melt comes in direct contact with the cold mold surface. The molecular orientation at the shear layer of the injection-molded products is due to the fountain-like flow at the melt front, which orients the polymer molecules in the flow direction parallel to the mold surface. In the center of the mold cavity, however, it has been found that the shear flow dominates in orienting the polymer molecules, but also, the packing and relaxation of chains due to longer cooling times give lower orientation.

Many authors have used different techniques to measure the variation of molecular orientation in the thickness direction of injection-molded products. Measurement of birefringence has been found to be the most accurate method, and the results indicate that the distribution of the orientation over the thickness of the part shows two maxima near the external surfaces, and a low orientation level in the core. According to Kamal and Tan,[19] the first minimum between these two maxima is associated with the skin layer, and the following maximum is associated with the shear/transcrystalline layer.

Excimer laser

Models for excimer laser surface modification

There are two basic mechanisms in laser-induced surface modification, thermal and photochemical, which are likely to take place simultaneously. The extents of these processes depend on the laser wavelength, frequency, intensity used, and the target material's properties.[20–22]

Details of excimer laser ablation mechanisms are still open to debate. Some authors have attributed ablation mainly to thermal decomposition, and others have attributed it to photochemical contribution.

Thermal and photochemical reactions are likely to both contribute, depending on the irradiation conditions and the type of polymer.

For irradiation of solids by laser frequencies corresponding to energies less than chemical bond strengths, it is obvious that one photon is incapable of directly forcing a molecule to undergo an electronic transition for bond breakage, but rather causing vibrations within the molecules. Consequently, material ablation is likely to correspond to evaporation rather than volume explosion.

Nonthermal laser ablation model

The basic principle involved in nonthermal ablation is that the laser photon energy is absorbed by the polymer, and it excites the electronic states that lie above the dissociation energy of the molecules.[23,24] The dissociation of molecular bonds leads to the splitting of longer polymer chains into small fragments. Numerous bond breaks cause an increase in pressure inside the laser-irradiated polymer volume, which causes the molecular fragments to escape. The extreme rapidity of the bond-breaking process eliminates heat conduction.[23]

Assuming that the ablation is a two-step process, in which the laser absorption is followed by material ablation, one can use the Beer–Lambert law to establish a relationship between the ablation depth per pulse (d_f), the absorption coefficient (α), the incident laser energy fluency (F_0), and the threshold energy fluency (F_T) as follows:

$$d_f = \left(\frac{1}{\alpha}\right) ln\left(\frac{F_0}{F_{th}}\right) \tag{1}$$

Thermal laser ablation model

In the thermal model, the incident laser energy is absorbed and then converted into thermal energy, which induces decomposition and chemical reactions. Thus, after the temperature profile is established, the decomposition reactions are assumed to take place. A first-order dissociation is usually assumed, and the temperature dependence of heat capacity is neglected.

Sancaktar and coworkers[25,26] defined the threshold intensity for degradation (I_d) as the laser intensity needed to create the degradation temperature (T_d) on the substrate surface. To estimate the threshold intensities, it was assumed that the phase transition was induced by the laser energy absorbed after the initiation of surface degradation. For a given pulse duration, I_d is given by

$$I_d = \frac{d_f \rho \Delta H_{\text{deg}}}{(1 - R)t'} \tag{2}$$

where d_f is the ablation depth (m), ΔH_{deg} is the heat of degradation (J/g), R is the reflectivity, and t' is the ablation time (s), defined as $t' = \tau - t_d$, where τ is the

duration of the laser pulse and t_d is the threshold duration for degradation. t_d is

$$t_d = \frac{\pi}{4D}\left[\frac{K(T_d - T_0)}{I(1-R)}\right]^2 \quad (3)$$

where T_d is the degradation temperature of the material (K) and T_0 is room temperature (K).

The total ablation depth (d_{total}) due to multiple laser pulses is given approximately as

$$d_{\text{total}} = nd_f \quad (4)$$

or

$$d_{\text{total}} = \frac{M}{wl\rho} \quad (5)$$

where n is the number of pulses, M is the ablated mass (g), w is the ablation width (m), l is the ablation length (m), and ρ is the density (g/m^3).[25,26]

The incident laser power intensity (I) for a laser pulse (τ = 25 ns) is given as follows:

$$I = \frac{E}{S\tau} \quad (6)$$

where E is the laser pulse energy (J) and S is the beam area (m^2). This equation does not include the plasma shielding effects induced by melting and ablation.

Factors affecting laser surface treatment

Different laser conditions provide different treatments on surfaces. A high frequency usually increases the thermal effect of lasers on the polymer. Therefore, at high frequency, a photothermal rather than photochemistry model is used to explain the ablation phenomena.[27–29]

The pulse number is an important factor in laser surface treatment. With increasing number of laser pulses, the ablation depth increases, and sometimes, the ripple structures formed become larger, and the distance between them increases.[30–32]

The pulse energy also plays an important role in surface treatment. Under different pulse lengths, the threshold energies of materials are different because the α for materials under different pulse lengths is different. The relationship between α and F_{th} was discussed by D'Couto et al.,[33] who reported that F_{th} usually decreases with increasing α. When the laser energy is under the F_{th} level, no obvious ablation occurs, but some structures may form on the polymer surface. When E is higher than F_{th}, ablation occurs at increasing levels with increasing pulse energy.[34,35]

Because materials absorb different amounts of energy at different wavelengths, laser wavelength is an important criterion that should be considered for surface modification applications.

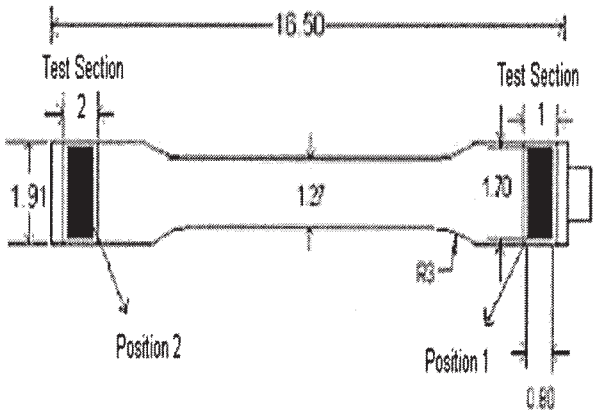

Figure 1 Positions (1 and 2) of ablation on an injection-molded dumbbell-shaped tensile specimen (all dimensions are in centimeters).

It is well known that the existence of threshold fluency is a main characteristic of the UV-laser-induced ablation of polymer surfaces. For a given α, the existence of a fluency threshold indicates that a specific minimum energy density is required for surface alteration.[36,37]

EXPERIMENTAL

Model materials

The materials used for this research were PET (Voridian PET 7352 Natural, Kingsport, TN); PBT (Crastin S610 NC010), 15% glass-filled PBT (Crastin SK602 NC010), 30% glass-filled PBT (Crastin SK605 NC010), all from DuPont (Wilmington, DE); PS (Styron Dow Chemical, Midland, MI); and PC (tradename Lexan, General Electric, Pittsfield, MA).

Experiments

Sample preparation

The injection molding of standard ASTM tensile bars for the aforementioned materials was done at different processing parameters (namely, varying injection speeds, pressures, and mold temperatures for neat materials and injection speeds, back pressures, and screw speeds for glass-filled materials).[38] To study the effect of stress relaxation and crystallinity, annealing was done for PET samples with a vacuum oven at three temperatures with a series of time intervals for each annealing temperature.

Laser ablation

Ablation of the molded and annealed tensile specimens was carried at two positions (positions 1 and 2,

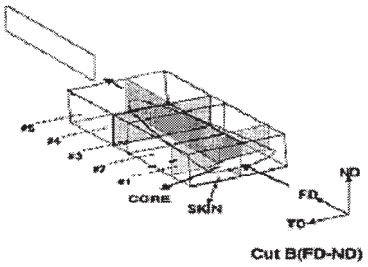

Figure 2 Sample cutting procedure for birefringence measurements.

Fig. 1) with predetermined laser parameters out in air. A Lambda Physik excimer laser (LPX 240i; Fort Lauderdale, FL) was used to treat the specimen surfaces at a wavelength of 248 nm (KrF). The KrF excimer laser produced laser pulses about 25 ns in duration. The dimensions of the unfocused beam were about 19.5 $\times$ 7 mm. The variation in power intensity across the laser beam cross-section resulted in variations in the ablation patterns obtained on specimen surfaces. Consequently, care was taken to confine the thermal measurement samples to the center of the ablation area. Specimen surfaces were treated under different numbers of pulses, pulse energies, and frequencies. Sample surfaces were perpendicular to the direction of the laser beam. The ablation effects were observed by investigation of the weight loss of the samples after ablation. The weight loss after ablation was measured with a digital balance (Mettler Toledo AX 205, Columbus, OH) with a resolution of 10 μg. Ablation depth values were measured with a Hommel T500 profilometer (VS-Schweningen, Germany).

Testing and analysis

The ablated surfaces were tested physically by ablation weight loss measurements with a weight balance. The determination of percentage crystallinity was carried out for the skin and core layers at positions 1 and 2 and, for all the molded and annealed samples, with DSC.

DSC

To determine the percentage crystallinity of the injection-molded and annealed PET samples, DSC analysis was done. Samples were taken from positions 1 and 2 of the dumbbell-shaped specimens. The skin and core regions were analyzed at both of these positions with 3–8 mg samples in each case. The heating ramp used from T_0 to 300°C was 15°C/min. The instrument used was a TA Instruments, Inc., model MDSC 2920 V2.6A (New Castle, DE). The mass fraction of the crystalline phase for a particular polymer was calculated with the following expression:[39]

$$X_c = (\Delta H_{\text{melt}} - \Delta H_{\text{crys}})/\Delta H^o \quad (7)$$

where ΔH_{melt} is the heat of fusion for melting from the DSC scan, ΔH_{crys} is the heat of fusion for crystallization from the DSC scan, and ΔH^0 is the heat of fusion for the 100% crystalline polymer (ΔH^0 = 115 J/g for PET).

Birefringence

Birefringence measurements were carried out on injection-molded PS and PC samples along the thickness direction with an optical microscope. The samples were prepared with a diamond-cutting saw. The samples were sectioned parallel to the flow direction (B-cut) in the flow direction–normal direction (FD-ND) plane, along the center at two positions, near the gate and near the end. The sample cutting procedure is shown in Figure 2. The samples were approximately 435 μm thick (transverse direction [TD]), 3.2 mm wide (ND), and 17 mm long (FD).

Annealing

Because PET-I samples were molded near standard and optimized conditions (see Table I), PET-I was selected for annealing studies. Samples were annealed in a vacuum oven, the same one used for material drying. The annealing temperatures were 100, 122, and 150°C. Six to seven samples were kept in the oven at the annealing temperature, and after a predetermined time interval, samples were taken out and quenched in cold water. Special holding plates were prepared to keep the dumbbell-shaped samples straight to prevent them from bending at higher temperatures in the oven and also while the samples were removed.

RESULTS AND DISCUSSION

Weight-loss measurements for PET

The summary of weight loss measurements due to laser ablation on the PET samples is given in Table I

TABLE I
Weight Loss Measurement Results for Injection-Molded PET Samples

Sample [mold temperature (°C), flow rate (cm^3/s)]	Weight loss (μg/100 pulses)	
	Position 1	Position 2
PET-I (20, 3.58)	1010	1000
PET-III (60, 3.58)	990	980
PET-IV (40, 118.8)	970	960
PET-V (40, 3.58)	1000	1000
PET-VII (25, 138.5)	960	960
PET-VIII (25, 73.27)	960	960
PET-IX (25, 8.54)	980	970

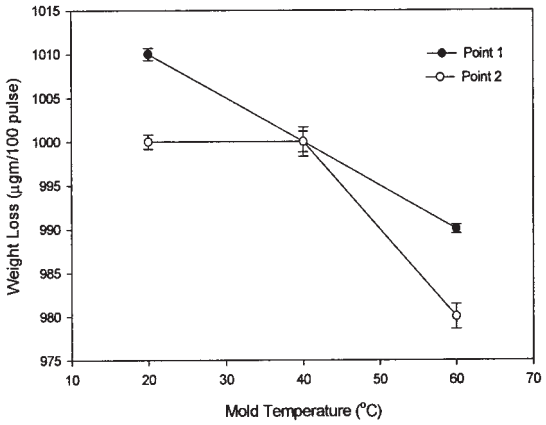

Figure 3 Effect of mold temperature on weight loss due to laser ablation for positions 1 and 2 on PET samples (flow rate = 3.58 cm^3/s).

for different processing conditions. Each value is an average of three readings and is rounded off to the nearest second digit (i.e., multiples of 10). Before the discussion on weight loss data, it is important that we note some aspects of this experimentation. To ensure significant weight loss, a higher laser fluence of 200 mJ/cm^2 was used, and the sample area was exposed to laser ablation for 3200 pulses. Depth measurements revealed that all of the ablation depths were in the range 19–24 μm, which gave us an ablation depth value of approximately 0.11 μm/pulse at a 200-mJ/cm^2 fluence. This meant that during the weight loss measurements, we reached a depth of approximately 320–350 μm from the surface.

Considering the thickness of the dumbbell-shaped specimen (3.2 mm), we calculated the frozen layer thickness as 160 μm with Mold Flow software (Mold Flow Corp., Framingham, MA). This indicated that in many of the weight loss measurements, we had penetrated the skin layer very well and were in the core region.

As shown in Figure 3, weight loss due to laser ablation decreased with increasing mold temperature. This could have been related to increases in the percentage crystallinity of the skin and core regions with increasing mold temperature for both positions 1 and 2. The summary of DSC analysis results for percentage crystallinity for all of the PET injection-molding conditions is given in Table II. As shown in Table II, the percentage crystallinity increased with increasing mold temperature. As the mold temperature increased, the time taken to freeze (cool) the polymer melt in the cavity increased. This gave more time for the polymer chains to crystallize, which resulted in a higher percentage crystallinity at higher mold temperatures.

The percentage crystallinity for the core region was much higher than that of the skin layer for all conditions. This was because the skin layer came directly in contact with the mold surface, which was at a much lower temperature; it froze instantly, which gave much less time for the chains to crystallize. On the other hand, the core region took a long time to freeze due to the poor thermal conductivity of the frozen skin layer, which resulted in much higher values of percentage crystallinity for the core region. Position 2 showed a higher percentage crystallinity for the skin region compared with the skin layer at position 1, which could have been due to stress-induced crystallization (the flowing polymer melt had to travel a longer distance under stress before solidifying). The core region, on the other hand, showed a higher percentage crystallinity for position 1 than for position 2.

The effect of flow rate on percentage crystallinity was not as pronounced as that of mold temperature.

Figure 3 reveals that position 1 had a higher weight loss than position 2, meaning that position 1 was more easily ablated. On the basis of the Mold Flow results we obtained, the frozen layer fraction for position 1 of all these three mold-temperature conditions (i.e., 20, 40, and 60°C) was about 0.4, whereas the frozen layer fraction for position 2 was about 0.1. As shown by the DSC results, the core region showed a much higher percentage crystallinity than the skin layer for all of the previous data. Thus, for position 2, we can state that because the laser ablation had crossed the frozen layer and was into the core region with a higher percentage crystallinity, there was greater resistance to ablation. For position 1, the majority of ablation took place in the lower percentage crystallinity frozen region. This may have been the reason for higher ablation weight loss for position 1 as compared with position 2.

Figures 4 and 5 show the effect of injection flow rate on ablation weight loss for mold temperatures of 40 and 25°C, respectively. Both plots showed an insignificant differences in positions 1 and 2 at all of the injection flow rates. At both mold temperatures, there was a decrease in weight loss due to ablation with increasing flow rate. This was expected because there

TABLE II
DSC Analysis Results for Injection-Molded PET Samples

Sample [mold temperature (°C), flow rate (cm^3/s)]	Crystallinity (%)			
	Position 1		Position 2	
	Skin	Core	Skin	Core
PET-I (20, 3.58)	2.56	6.03	3.38	4.90
PET-III (60, 3.58)	11.63	29.46	12.05	20.33
PET-IV (40, 118.8)	8.22	13.83	9.26	13.06
PET-V (40, 3.58)	8.89	17.41	11.44	16.92
PET-VII (25, 138.5)	10.32	10.98	10.56	10.83
PET-VIII (25, 73.27)	7.64	11.74	8.82	11.18
PET-IX (25, 8.54)	6.98	13.06	7.15	12.80

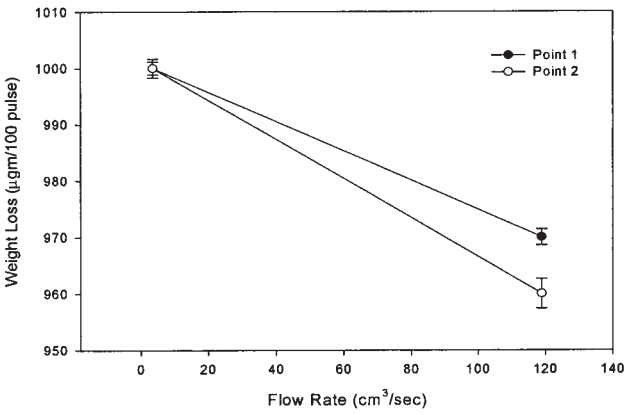

Figure 4 Effect of flow rate on weight loss due to laser ablation for positions 1 and 2 on PET samples (mold temperature = 40°C).

was a large decrease in the frozen layer fraction with increasing flow rate. Therefore, the core region with a higher percentage crystallinity than the skin layer got exposed earlier if molded at higher flow rates and thus acquired a higher resistance to the laser ablation. This provided a lower weight loss for samples molded at higher flow rates.

Table III gives the summary of weight loss due to the laser ablation of annealed PET-I samples. The weight loss due to laser ablation decreased with increasing annealing time at all of the annealing temperatures. This was quite expected because the percentage crystallinity increased with increasing annealing time for both positions 1 and 2 and, thus, decreased ablation. The differences in the percentage crystallinity and residual stress levels between the skin and core layers were decreased considerably with annealing.

Weight-loss measurements for PBT

Weight loss measurements were taken for all neat and glass-filled PBT samples. Table IV gives the summary of weight loss measurements.

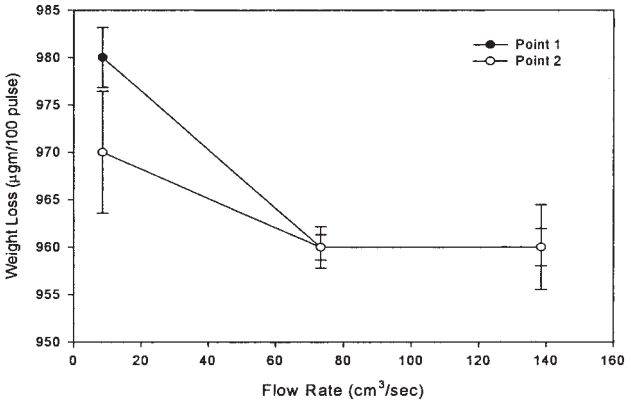

Figure 5 Effect of flow rate on weight loss due to laser ablation for positions 1 and 2 on PET samples (mold temperature = 25°C).

TABLE III
Weight Loss Measurement Results for Annealed PET-I Samples

Annealing temperature (°C)	Annealing time (min)	Weight loss (μg/100 pulses)	
		Position 1	Position 2
100	0	1010	1000
	30	990	980
	60	980	970
	120	995	980
	240	965	970
	360	965	975
	420	965	975
122	0	1010	1000
	10	990	985
	15	990	985
	30	985	990
	45	985	995
	120	985	990
	200	980	980
	260	980	990
150	0	1010	1000
	4	995	985
	5	985	990

Figure 6 shows the effect of injection flow rate on the weight loss due to laser ablation for neat PBT samples.

The effect of increasing injection pressure is also shown in Table IV, and the results indicate that the weight loss due to laser ablation decreased with increasing injection and holding pressure. This was attributed to a higher packing of material at higher injection pressures.

As expected, PBT also showed a reduction in weight loss for neat and glass-filled samples due to ablation with increasing flow rate, and the difference between

TABLE IV
Summary of Weight Loss Measurements for Neat and Glass-Filled PBT Samples

Sample [flow rate (cm³/s), injection pressure (psi), screw speed (rpm)]	Weight loss (μg/100 pulses)	
	Position 1	Position 2
PBT-I (17.08, 700, 120)	645	640
PBT-II (73.27, 700, 120)	605	610
PBT-III (138.50, 700, 120)	620	625
PBT-IV (138.08, 2000, 120)	605	610
PBT-V (17.08, 2000, 120)	595	595
PBT 602-I (17.08, 700, 75)	620	420
PBT 602-II (138.50, 700, 75)	410	420
PBT 602-III (17.08, 700, 400)	415	410
PBT 602-IV (17.08, 2000, 400)	420	410
PBT 605-I (17.08, 700, 75)	265	260
PBT 605-II (138.50, 700, 75)	265	255
PBT 605-III (17.08, 700, 400)	255	260
PBT 605-IV (17.08, 2000, 400)	260	270

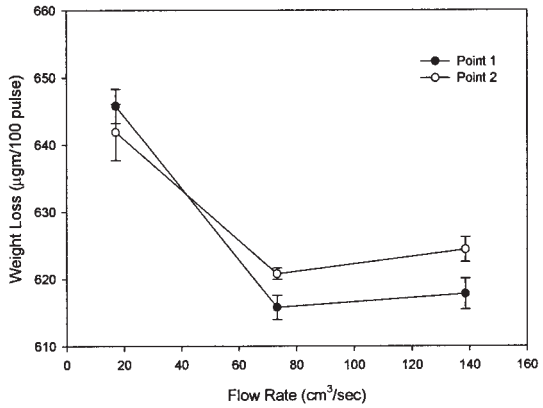

Figure 6 Effect of injection flow rate on weight loss due to laser ablation for neat PBT samples.

positions 1 and 2 was small. There was a drastic decrease in weight loss with increasing glass fiber content for both positions 1 and 2.

A comparison between the experimental and calculated weight loss values clearly indicated a shielding effect by the exposed glass fibers on laser irradiation. In comparison to the calculated values, the experimental results showed about a 28% reduction in weight loss for 15% glass-filled samples and about 50% for 30% glass-filled samples (Table V). This clearly indicated that once directly exposed to laser irradiation, the dispersed glass fibers shielded some of the underlying resin from further ablation. This shielding effect was obviously larger than what would be predicted on the basis of glass fiber volume fraction alone.

Scanning electron microscopy (SEM) of PBT

Figure 7 shows SEM images of the ablated samples of 15% glass-filled PBT. It is clearly shown in these pictures that more fibers were oriented in flow direction for position 2 than for position 1.

Fiber angle measurements

Scion image analysis software (by Scion Corp., Frederick, MD) was used to determine the fiber angles with

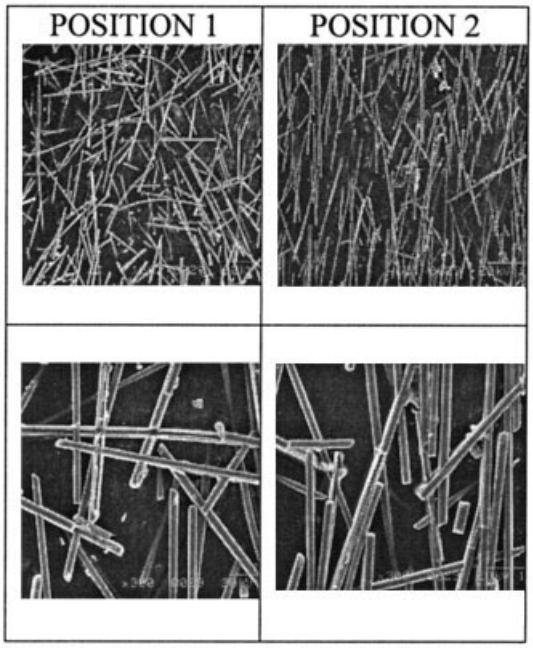

Figure 7 SEM images of laser-ablated PBT 602-I.

respect to flow direction in the SEM pictures with magnification of 60×. About 100–110 fiber angles were measured in each image. The result summary for average fiber angle is given in Table VI along the standard deviation values. In this analysis, 0° corresponds to the flow direction.

As shown in Table VI, position 2 showed lower standard deviations for all samples. This meant that more fibers had angles near zero or flow direction. In other words, position 2 had a higher orientation in the flow direction than position 1. This was also shown in the mold flow analysis results with the values of fiber orientation tensor being higher for position 2 than position 1.

Birefringence measurements on PS and PC

Birefringence measurements were carried out on injection-molded PS and PC samples along the thickness

TABLE V
Calculated Weight Loss Based on the Resin Volume Fraction

Sample [flow (cm^3/s), injection pressure (psi)]	Experimental weight loss (μg/100 pulses)				Weight loss calculated with the resin volume (μg/100 pulses)	
	Position 1	Position 2	Fiber (wt %)	Resin (vol %)	Position 1	Position 2
PBT-I (17.08, 700)	645	640	0	100	645	640
PBT 602-I (17.08, 700)	420	420	15	91.5	590	586
PBT 605-I (17.08, 700)	265	260	30	81.77	527	523
PBT-III (138.5, 700)	620	625	0	100	620	625
PBT 602-II (138.5, 700)	410	420	15	91.5	567	572
PBT 605-II (138.5, 700)	265	255	30	81.77	507	511

TABLE VI
Average Fiber Angles for PBT 602 Samples

Sample	Position	Average fiber angle	Standard deviation
PBT 602-I (17.08, 700, 75)	1	−17.06	46.54
	2	−12.05	28.37
PBT 602-II (138.5, 700, 75)	1	0.77	39.14
	2	2.36	26.31
PBT 602-III (17.08, 700, 400)	1	−14.81	41.23
	2	−3.37	24.36
PBT 602-IV (17.08, 2000, 400)	1	−3.06	35.96
	2	−3.83	26.02

direction with an optical microscope. The values of birefringence for PS were negative as PS was a negatively birefringent material, whereas PC, being positively birefringent, had positive birefringence values. Both PS and PC exhibited dog-ear birefringence profiles across the thickness with maximum birefringence at intermediate regions close to the skin. The center of the parts exhibited little or no birefringence compared to the skin. This was due to the rapid decay of stresses and orientation developed as a result of slow cooling along the core. The values of the maximum birefringences for different injection-molding conditions are summarized in Table VII for PS and in Table VIII for PC. As shown in Tables VII and VIII, an increase in the injection flow rate led to a decrease in the value of the maximum birefringence at comparable injection pressure and mold temperature values. This was because increasing the flow rate led to a truncation of the long-term tail of the relaxation spectrum for the polymer melt and, thus, reduced the effective relaxation time. The second reason was that at high flow rates, thermal convection dominated over thermal conduction to the cold mold and, thus, created favorable conditions for the relaxation process and retarded the growth of the frozen surface layer. This retardation in the frozen surface layer with injection flow rate was also observed in the mold flow analysis carried out on the samples and as shown in Tables VII and VIII for PS and PC, respectively. Furthermore, an increase in mold temperature resulted in a decrease in the value of the birefringence at comparable injection flow rates and injection pressure values due to the reduction in effective relaxation time. An increase in injection pressure at comparable injection flow rate and mold temperature values, however, led to an increase in the value of the birefringence, which was possibly due to higher stress gradients. For all conditions, the birefringence decreased with increasing distance from the gate. Around the gate area, the skin layer was in contact with the cold cavity wall longer than away from the gate in the filling stage. Thus, the solidified melt was thicker near the gate, which resulted in a larger birefringence value.

TABLE VII
Maximum Birefringence for the PS Samples at Different Positions

Sample [flow (cm^3/s), pressure (MPa), mold temperature (°C)]	Position 1 [$\times(-1 \times 10^{-6})$]	Position 2 [$\times(-1 \times 10^{-6})$]
PS-I (13.5, 5.5, 25)	3172	2080
PS-II (73, 5.5, 25)	2660	2213
PS-III (137, 5.5, 25)	1774	701
PS-IV (137, 13.8, 25)	1952	1654
PS-V (137, 5.25, 25)	3623	2128
PS-VI (137, 5.25, 40)	3108	2109
PS-VII (137, 5.25, 65)	1496	982

TABLE VIII
Maximum Birefringence for PC Samples at Different Positions

Sample [flow (cm^3/s), pressure (MPa), mold temperature (°C)]	Position 1 ($\times 10^{-6}$)	Position 2 ($\times 10^{-6}$)
PC-I (9.8, 5.5, 50)	3379	2249
PC-II (97.8, 5.5, 50)	2370	1153
PC-III (137, 5.5, 50)	1391	680
PC-IV (9.8, 13.8, 50)	3786	708
PC-V (137, 5.5, 80)	667	660
PC-VI(137, 5.5, 125)	505	672

Weight loss of PS and PC due to laser irradiation

The weight loss results for different injection-molding conditions for PS are summarized in Table IX.

The weight loss increased with increasing injection flow rate for both positions 1 and 2. For position 1, there was an increase in the weight loss of 12.25% as the injection flow rate increased from 13.5 to 73 cm^3/s, which was followed by a very gradual increase of 0.3% as the injection flow rate increased from 73 to 137 cm^3/s.

TABLE IX
Weight Loss Results for PS

Sample [flow (cm^3/s), pressure (MPa), mold temperature (°C)]	Weight loss (μg/100 pulses)	
	Position 1	Position 2
PS-I (13.5, 5.5, 25)	231	230
PS-II (73, 5.5, 25)	260	246
PS-III (137, 5.5, 25)	261	257
PS-IV (137, 13.8, 25)	258	256
PS-V (137, 5.25, 25)	251	233
PS-VI (137, 5.25, 40)	257	238
PS-VII (137, 5.25, 65)	265	239

TABLE X
Weight Loss Results for PC

Sample [flow (cm^3/s), pressure (MPa), mold temperature (°C)]	Weight loss ($\mu g/100$ pulses)	
	Position 1	Position 2
PC-I (9.8, 5.5, 50)	468	463
PC-II (97.8, 5.5, 50)	474	465
PC-III (137, 5.5, 50)	475	466
PC-IV (9.8, 13.8, 50)	468	465
PC-V (137, 5.5, 80)	477	469
PC-VI (137, 5.5, 125)	485	464

Position 1 showed a higher weight loss compared to position 2 for all of the injection flow rates. The weight loss showed a decrease of 0.9% for position 1 and 0.4% for position 2 with increasing injection pressure from 5.5 to 13.8 MPa. Also, weight loss increased with increasing mold temperature for both positions 1 and 2. Position 1 showed a higher weight loss compared to position 2 for all of the mold temperatures.

These results for the effect of injection-molding conditions on weight loss for PS were consistent with our earlier findings on birefringence. An increase in the injection flow rate for PS resulted in a decrease in the birefringence values. A similar effect was observed for mold temperature. A decrease in birefringence led to a decrease in the orientation of the polymer chains, which in turn, implied a less compact arrangement of the polymer chains, and hence, they could be ablated more easily. An increase in injection pressure led to higher birefringence and, hence, lower weight loss values. The higher weight loss at position 1 compared to position 2 was attributed to the higher residual stresses at position 1 than at position 2.

The weight loss results for different injection-molding conditions for PC are summarized in Table X.

The weight loss increased with increasing injection flow rate for both positions 1 and 2. The weight loss at position 1 showed an increase of 2% as the injection flow rate increased from 9.8 to 97.8 cm^3/s and, then, a gradual increase of 0.2% as the injection flow rate increased from 97.8 to 137 cm^3/s. Position 1 showed a higher weight loss compared to position 2 for all injection flow rates.

The weight loss at position 1 showed a slight decrease with injection pressure (0.1%), whereas position 2 showed a slight increase (0.5%). Increases in mold temperature resulted in an increase in weight loss at position 1, whereas with changes in mold temperature, position 2 did not show any change.

CONCLUSIONS

Weight loss due to laser ablation depended on the morphology of the skin and core regions. It also varied with the frozen layer fraction. For PET, weight loss decreased with increasing mold temperature and remained insensitive to injection flow rate. Annealing time and temperature significantly reduced weight loss. Thus, we concluded that crystalline zones/crystals could resist laser irradiation to a greater extent when compared to amorphous regions for PET.

For PBT, the weight loss due to laser ablation decreased with increasing material packing due to pressure. Also, it showed some sensitivity to flow rate variation. The major effect was seen with glass-filled PBT samples. The weight loss reduced drastically with increasing glass fiber content. There was a shielding effect by the exposed glass fibers on laser irradiation. This shielding effect was larger than what would be predicted on the basis of glass fiber volume fraction alone. The profile scan perpendicular to the flow direction showed a larger disturbance compared to that in the flow direction due to fiber orientation in the flow direction. Scion image analysis and mold flow analyses showed higher fiber orientation in flow direction at the end position of the specimen (position 2) compared with the gate region (position 1).

For PS, weight loss increased with increasing flow rate and mold temperature for both the gate and end positions. The weight loss showed a decrease of 0.9% for the gate position and 0.4% for the end position with increasing injection pressure from 5.5 to 13.8 MPa for PS. For PC, weight loss at the gate position showed an increase of 2% as the injection flow rate increased from 9.8 to 97.8 cm^3/s and, then, a gradual increase of 0.2% as the injection flow rate increased from 97.8 to 137 cm^3/s. For PC, increasing mold temperature resulted in increasing weight loss for the gate position, whereas no specific trend was observed for the end position. The change in weight loss with injection pressure for PC was not consistent.

The excimer laser used in this work was acquired with the financial assistance of the National Science Foundation.

References

1. Johannaber, F. Injection Molding Machines: A User's Guide; Hanser: New York, 1994.
2. Brent, S. Plastics: Materials and Processing, 2nd ed.; Prentice Hall: Upper Saddle River, NJ, 2000.
3. Rosato, D.; Rosato, D. Injection Moulding Handbook: The Complete Molding Operation; Van Nostrand Reinhold: New York, 1986.
4. Tadmor, Z.; Gogos, C. G. Principles of Polymer Processing; Wiley-Interscience: New York, 1979.
5. Katti, S. S.; Schultz, J. M. Polym Eng Sci 1982, 22, 1001.
6. Ulcer, Y. Ph.D. Thesis, University of Akron, 1995.
7. Hsiung, C. M.; Cakmak, M.; Ulcer, Y. Polymer 1996, 37, 4555.

8. Spruiell, J. E.; White, J. L. Polym Eng Sci 1975, 15, 660.
9. Hsiung, C. M.; Cakmak, M.; White, J. L. Int Polym Process 1990, 5, 109.
10. Guo, X. Ph.D. Thesis, University of Akron, 1999.
11. Daly, H.; Nguyen, K.; Sanschagrin, B.; Cole, K. J Injection Molding Technol 1998, 2, 59.
12. Ezrin, M. Plastics Failure Guide; Hanser: New York, 1996.
13. Dally, J. W.; Ripley, W. F. Experimental Stress Analysis; McGraw-Hill: New York, 1991.
14. Kantz, M. R.; Newman, H. D.; Stigale, F. H. J Appl Polym Sci 1972, 16, 1219.
15. Kantz, M. R. Int J Polym Mater 1974, 3, 245.
16. Sanchez, L. A.; Hornberger, L. E. Opt Lasers Eng 2002, 37, 27.
17. Isayev, A. I.; Hieber, C. A. Rheol Acta 1980, 19, 168.
18. Fernandez, M. R.; Merino, J. C.; Pastor, J. M. Polym Eng Sci 2000, 40, 95.
19. Kamal, M.; Tan, V. Process Int Conf 1979, 665.
20. Von Allmen, M. In Laser and Electron Beam Processing of Materials; White, C. W.; Peercy, P. S., Eds; Academic: San Diego, 1980; p 6.
21. Wood, R. F.; Wang, J. C.; Giles, G. E.; Kirkpatrick, J. R. In Laser and Electron Beam Processing of Materials; White, C. W.; Peercy, P. S., Eds.; Academic: San Diego, 1980; p 37.
22. Breinan, E. M.; Kear, B. H. In Laser Materials Processing; Bass, M., Ed.; Elsevier: Amsterdam, 1983; p 235.
23. Sentrayan; Thorpe; Trouth. Spectrosc Lett 1998, 31, 559.
24. Park, J. K.; Mukherjee, K. Mater Manufacturing Process 1998, 13, 359.
25. Sancaktar, E.; Zhang, E. In Reliability, Stress Analysis, and Failure Prevention Aspects of Composite and Active Materials; Sancaktar, E.; Lee, J. S., Eds; American Society of Mechanical Engineers: New York, 1994; Vol. 79, p 65.
26. Sancaktar, E.; Babu, S. V.; Zhang, E.; D'Couto, G. C. J Adhes 1995, 50, 103.
27. Hopp, B.; Bor, Z.; Homolya, E.; Mihalik, E. Appl Surf Sci 1997, 109, 232.
28. Kesting, W.; Knittel, D. Angew Makromol Chem 1991, 191, 145.
29. Knittel, D.; Schollmeyer, E. Polym Int 1998, 45, 103.
30. Knittel, D.; Kesting, W.; Schollmeyer, E. Polym Int 1996, 43, 231.
31. Cain, S. R.; Burns, F. C. J Appl Phys 1992, 71, 4107.
32. Deutsch, T. F.; Greis, M. W. J Appl Phys 1983, 54, 7201.
33. D'Couto, G. C.; Babu, S. V.; Egitto, F. D.; Davis, C. R. J Appl Phys 1993, 74, 5972.
34. Knittel, D.; Kesting, W.; Bahaners, T.; Schollmeyer, E. Appl Surf Sci 1992, 54, 330.
35. Krajnovich, D. J.; Vazquez, J. E. J Appl Phys 1993, 73, 3001.
36. Sancaktar, E.; Lu, H. In Polymer Surface Modification: Relevance to Adhesion; Mittal, K. L., Ed.; VSP: Utrecht, The Netherlands, 2004; Vol. 3, p 183.
37. Sancaktar, E.; Sunthonpagasit, N. In Polymer Surface Modification: Relevance to Adhesion; Mittal, K. L., Ed.; VSP: Utrecht, The Netherlands, 2004; Vol. 3, p 285.
38. Sancaktar, E.; Negandhi, N.; Adwani, S. In Proceedings of the 2004 ASME International Mechanical Engineering Congress and Exposition [CD-ROM]; Sancaktarm, E., Ed.; American Society of Mechanical Engineers: New York, 2004; Vol. 2, Paper IMECE 2004–59356.
39. Kong, Y.; Hay, J. N. Polymer 2002, 43, 3873.